Journal of the European Ceramic Society 22 (2002) 1621–1629

www.elsevier.com/locate/jeurceramsoc

Quantitative EFTEM study of precursor-derived Si–B–C–N ceramics

Achim Zern[a,*], Joachim Mayer[a,1], Narayanan Janakiraman[b], Markus Weinmann[b], Joachim Bill[b], Manfred Rühle[b]

[a]*Max-Planck-Institut für Metallforschung, Seestr. 92, D-70174 Stuttgart, Germany*
[b]*Max-Planck-Institut für Metallforschung and Institut für nichtmetallische anorganische Materialien, Universität Stuttgart, Pulvermetallurgisches Laboratorium, Heisenbergstr. 5, D-70569 Stuttgart, Germany*

Received 8 June 2001; received in revised form 6 August 2001; accepted 15 August 2001

Abstract

Ceramic materials derived from a boron modified polysilazane were investigated by means of energy-filtering transmission electron microscopy (EFTEM). After cross-linking of the polymer and subsequent thermolysis, a coarse powder with average composition $Si_{24.0}B_{8.0}C_{44.0}N_{24.0}$ is obtained. For further investigation, monolithic particles with sizes of several millimeters were heat treated in crucibles under a flowing nitrogen atmosphere at 1800 °C for 10 h. During thermolysis, the particles developed internal cracks on the macroscopic scale. At the crack surfaces, a layer of pure carbon was found. In the crack-free region, the material is composed of Si_3N_4 and SiC nano crystallites which are embedded in a turbostratic BNC-matrix. Quantitative electron spectroscopic imaging (ESI) shows an atomic ratio of the elements B:C:N of 1.0:4.0:1.1 in this matrix. In the vicinity of the cracks, silicon nitride locally decomposes with formation of silicon carbide because of its reaction with excess carbon. A detailed EFTEM study of the phase distribution near the crack surfaces showed that the first Si_3N_4 crystallites occur at a distance of approx. 5 μm from the carbon covered crack surface. In additional experiments the composition of the BNC-layers as a function of the distance from the crack surface was investigated.

Keywords: EFTEM; Electron microscopy; Phase composition; Precursors:organic; Si–B–C–N

1. Introduction

Preparing ceramic materials from polymer precursors offers many advantages compared to the classical powder preparation route. Riedel et al.[1] showed that by direct transformation of organometallic precursors into non-oxide silicon-based ceramics, SiCN composites with densities up to 93% could be obtained. In contrast to the conventional powder metallurgical methods, no sintering additives, which form low melting oxygen-rich intergranular phases, are present in precursor-derived materials.[2] Furthermore, as was pointed out first by Niihara,[3] a large variety of different microstructures can be designed by choosing appropriate chemical composition and processing parameters for the polymers. Basic properties like temperature stability of the ceramics can be improved by the introduction of boron.[4–10] After cross-linking and thermolysis of boron-modified polysilazanes, an amorphous material is obtained which can subsequently be transformed into crystalline composites in an additional annealing step. The covalently bonded SiBCN material offers a high thermal stability and a high oxidation resistance.[10–12] However, since the polymer-to-ceramic conversion is always accompanied with the formation of volatile byproducts and shrinkage, crack- and pore-free bulk material is usually difficult to obtain.

From thermodynamic calculations,[13,14] it is expected that below a temperature of 1484 °C (1 atm N_2) a crystalline material with an overall composition $Si_{24.0}B_{8.0}C_{44.0}N_{24.0}$ is composed of 32 atom% C, 16 mol% BN, 28 mol% Si_3N_4 and 24 mol% SiC. Besides the two crystalline phases Si_3N_4 and SiC, a turbostratic BN C matrix phase with an atomic ratio of the elements B:N:C of 1.0:1.0:4.0 is expected. Further consideration

* Corresponding author.
E-mail address: zern@hrem.mpi-stuttgart.mpg.de (A. Zern).

[1] Now at Gemeinschaftslabor für Elektronenmikroskopie, RWTH Aachen, Ahornstr. 55, D-52074 Aachen, Germany.

0955-2219/02/$ - see front matter
PII: S0955-2219(01)00443-5

of the phase equilibria reveals that the presence of carbon in this BNC-matrix is connected with a quantitative decomposition of silicon nitride above 1484 °C according to:

$$Si_3N_4 + 3C => 3SiC + 2N_2.$$

Nevertheless, this particular ceramic material can be heat-treated at 1800 °C and we find the presence of Si_3N_4. These results are in agreement with TGA measurements (thermogravimetric analysis) showing no mass loss up to 2000 °C, which otherwise should accompany the degradation of silicon nitride.[12] Thus, the given phase composition was proven to be stable up to 2000 °C. Jalowiecki et al. found in SiBCN ceramics with 1 and 6 wt.% boron that turbostratic BN layers coating the Si_3N_4 crystallites and thus acting as a diffusion barrier for both the carbon and nitrogen.[15] Thus, the carbon activity decreases and the decomposition of Si_3N_4 is shifted to temperatures above 1484 °C. It has to be noted that this phenomenon was only observed in the center of compact particles, away from crack or surface areas. One aim of this paper is to study compositional deviations of bulk material from crack or surface near ceramic. The results indicate that surface effects and internal particle boundaries also play an important role in corrosion processes during both thermolysis and annealing whereby particularly smaller particles strongly suffer from the influence of boundaries.

In the present paper, we report on the detailed study of the boundary phenomena in these ceramics. We focus on internal boundary effects in a material with a chemical composition of $Si_{24.0}B_{8.0}C_{44.0}N_{24.0}$, which corresponds to a boron content of about 6 wt.%. Besides conventional transmission electron microscopy (TEM), energy filtering transmission electron microscopy (EFTEM) was used for characterization. The applied ESI methods use the characteristic inner shell energy loss edges for mapping the element distribution over large specimen areas (several square microns). The main advantage of these new EFTEM techniques over scanning techniques is that they are very time efficient, since just a few energy filtered images have to be recorded in order to obtain spatially resolved information on the elemental distribution in large specimen areas.[16]

2. Experimental

2.1. Sample preparation

The ceramic materials used in the present studies were obtained by hydroboration of oligovinylsilazane (OVS) and subsequent thermolysis as described recently by Weinmann et al. (the material investigated here is labelled '1P' in this publication).[12] Thermolysis was performed from 25 to 1400 °C using a heating rate of 1 °C/min and a dwell time of 3 h. The chemical composition of the '1P' ceramic after thermolysis determined by elemental analysis is $Si_{24.0}B_{8.0}C_{44.0}N_{24.0}$. The material described here was additionally annealed in a carbon crucible at a temperature of 1800 °C, where it is held for 10 h in a nitrogen atmosphere.

2.2. Transmission electron microscopy

A Zeiss EM 912 Omega was used for the experimental work. The instrument is equipped with an imaging omega filter and was operated at 120 kV. Elemental distribution images were obtained with the 'three window method'.[17] In this method, two images are taken in the structureless background of the EEL spectrum. Using these two images, the background can be extrapolated and subtracted from a third image which is acquired above the edge and contains the element specific signal. Energy window widths between 10 and 60 eV were chosen. See Table 1 for detailed information on window widths and positions. Elemental maps show the distribution of the element in the observed specimen area.

More quantitative information about the local chemical composition was gathered by acquiring electron spectroscopic image series. From these series it is possible to extract the electron energy loss spectrum (EELS) in the energy range of interest.[18,19] For acquiring the ESI series, an energy window with a width of 10 eV was swept over an energy range from 120 to 450 eV. In this energy range the boron K-edge (188 eV), the carbon K-edge (284 eV) and the nitrogen K-edge (401 eV) are present and can be quantified with the common tools for EELS analysis.

TEM specimens were prepared by polishing and dimpling. In the case of brittle and porous samples or single ceramic particles, alumina cross section holders were used to stabilize the sample material in the preparation steps. This preparation technique was developed by Strecker et al.[20] The final thinning to electron transparency was performed by Ar ion beam bombardment in a Baltec Res 010 at an angle of 6° and an ion energy of 5 keV.[21]

3. Experimental results

Fig. 1 shows the internal crack structure of a particle on a macroscopic scale, as revealed by optical microscopy. The spherical particle with a diameter of approximately 5 mm was ground and polished. The bright areas show the composite material, whereas the cracks appear as dark lines. By successively grinding into the particle, we were able to obtain information on the three- dimensional structure of the crack pattern.

Table 1
Window widths and positions used for the acquisition of the elemental maps

Element	Edge (eV)	Energy window width (eV)	Pre-edge 1 (eV)	Pre-edge 2 (eV)	Postedge (eV)
Boron	K, 188	10	168	178	193
Nitrogen	K, 401	30	351	381	416
Silicon	K, 1839	60	1744	1804	1869
Carbon	K, 284	20	239	269	299

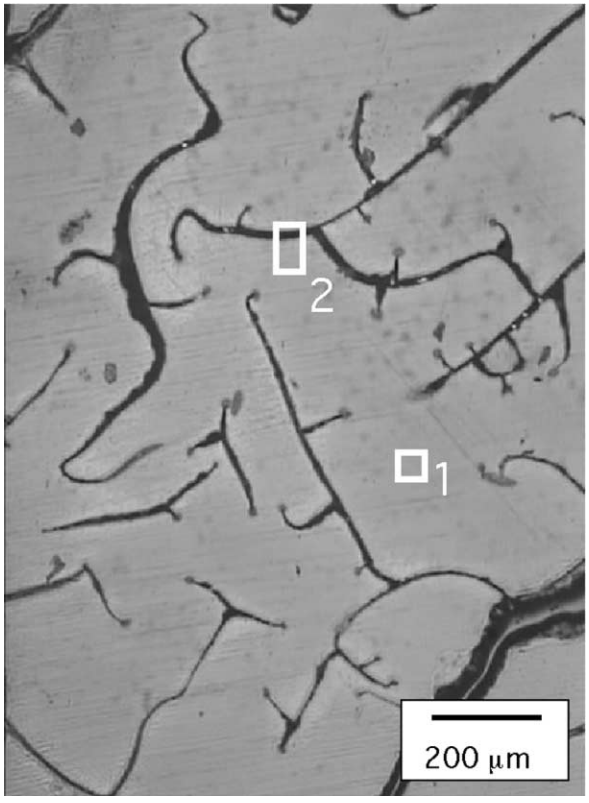

Fig. 1. Cross-section of the particle, showing the crack system on macroscopic scale.

The cracks are planar and connected to other cracks in an array of intersections, thus forming an interconnected network resulting in open porosity. Frequently, the cracks have smaller 'side arms' branching off at an angle of 90°. Two representative sample positions 1 and 2, indicated in Fig. 1, were analyzed in EFTEM in order to gather information about the elemental distribution and quantitative chemical composition. Position 1 characterizes the ceramic material far away from any crack, position 2 is located at a crack surface.

3.1. Position 1: bulk material at large distance from cracks

The TEM micrographs and elemental disribution images in Fig. 2 show the microstructure and composition of the annealed ceramic material at position 1 in Fig. 1. The elemental maps (b)–(e) depict the distribution of nitrogen, boron, carbon and silicon, which show that in this area silicon carbide and silicon nitride nanocrystallites are embedded in a turbostratic BNC matrix.

Since position 1 is far away from any crack surface, we expect a representative microstructure with the average chemical composition of the ceramic. Recording an ESI series and extracting EEL spectra at several different positions of the BNC matrix, a quantitative analysis of the atomic ratio of the elements B, N and C constituting the matrix phase could be performed. Fig. 3 shows an experimental spectrum, which was extracted from the image area indicated by the white rectangle shown in Fig. 2a. The steplike structure results from the energy window of 10 eV width which was used during acquisition of the ESI series. Consequently, the obtained EEL spectrum cannot resolve details below 10 eV energy resolution. For further evaluation, the spectrum was interpolated (also shown in Fig. 3) and evaluated with the Gatan ELP Software. We obtained an average atomic ratio B:C:N of 1.0:4.0:1.1 (±15%), which is in full agreement with the thermodynamic calculations based on elemental analysis which were reported by Weinmann et al.[12]

The grain size distribution at position 1 was evaluated quantitatively in the bright field images. A detailed view is shown in Fig. 2a. We measured a total of 212 grains. For each grain two perpendicular diameters were determined and averaged. Using the nitrogen and carbon maps shown in Fig. 2b and d, respectively, we also determined individual crystals. 99 silicon nitride crystals with an average grain size of 43 nm (±3%) were identified. The remaining 113 SiC crystals show an average grain size of 36 nm (±3%). This statistical error in the mean grain size originates from an estimated accuracy of ±30% in determining a single grain diameter. A further systematic error may result from the fact that grains could be cut, since the TEM specimen thickness is in the range of the grain size. This might shift the mean diameter to lower values but was not taken into account in the quantitative evaluation. Grain size distributions are shown in Fig. 4. By weighting the diameters to their third power a volume ratio of Si_3N_4:SiC of 1.07:1 (±20%) was obtained. Both silicon nitride and silicon carbide exhibit densities very close to 3200 kg/m^3.[22] Consequently mass- and volume fraction are

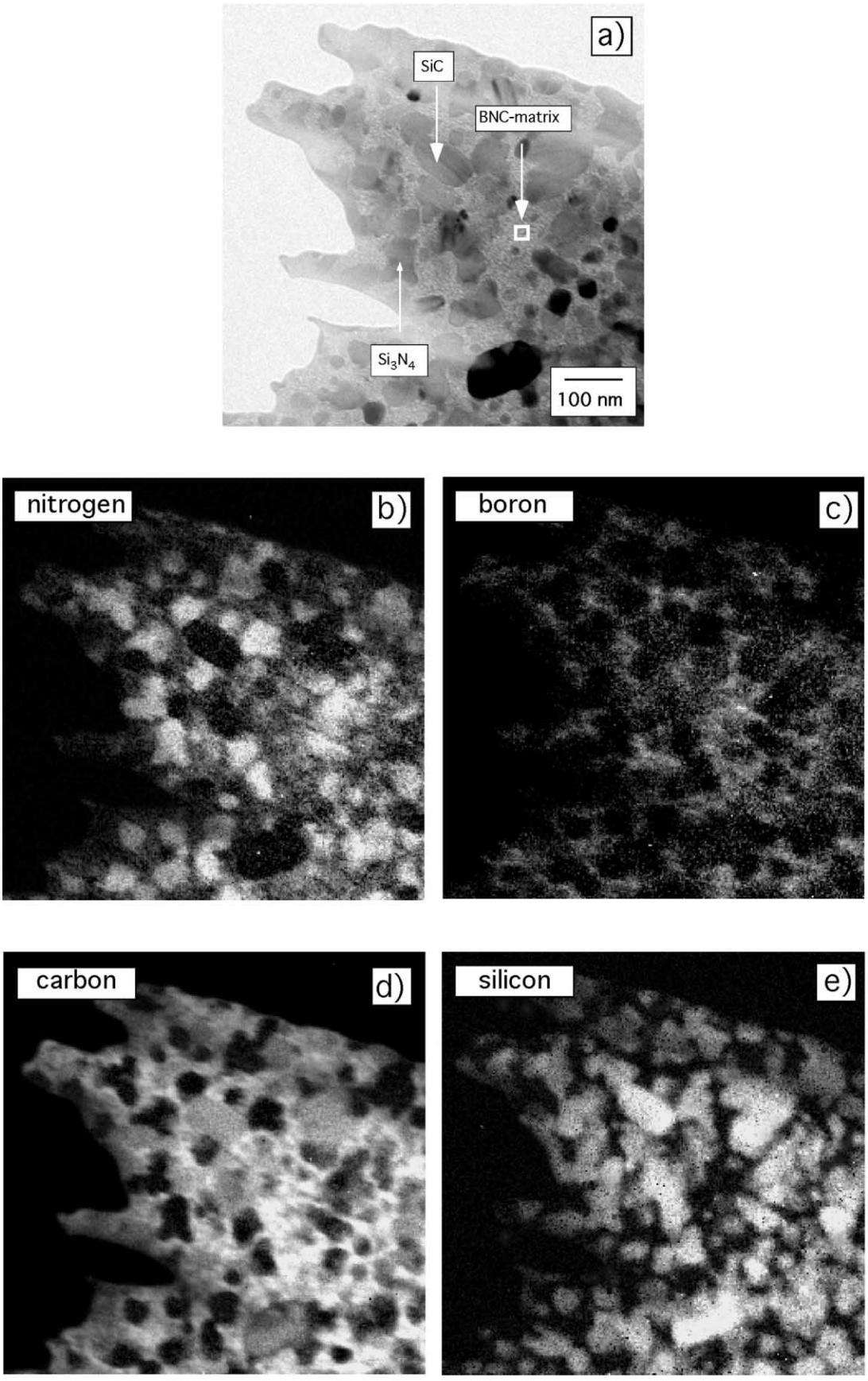

Fig. 2. Elemental maps of the ceramic at position 1: (a) bright field image, (b) nitrogen, (c) boron, (d) carbon and (e) silicon.

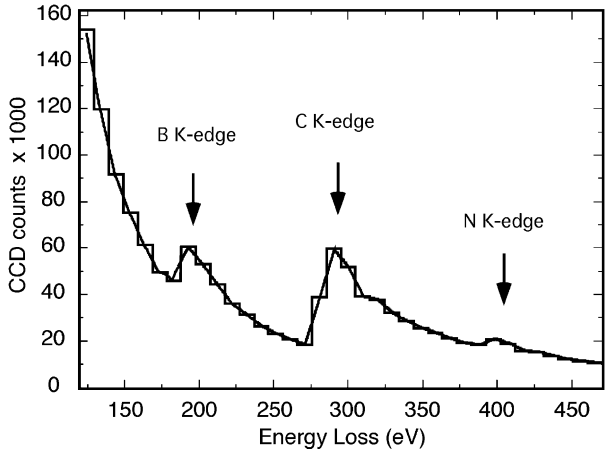

Fig. 3. Characteristic EEL spectrum of the BNC matrix extracted from an ESI series by integrating the signal in an area of 20×20 nm^2.

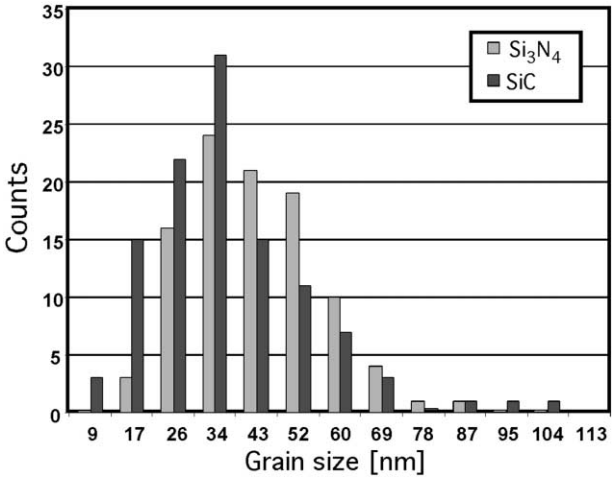

Fig. 4. Grain size distributions at position 1: average grain size of Si_3N_4 43 and SiC 36 nm.

almost similar. This experimentally determined value is in good agreement with the mass ratio of silicon nitride to silicon carbide of 1.17:1 obtained by thermodynamical calculation.

3.2. Position 2: structure in the vicinity of a crack

Position 2 is located close to a crack, where a much more complex microstructure compared to that of position 1 is observed. We have to distinguish between four laterally preceding microstructures which occur with increasing distance from the crack:

I. At the crack surface, indicated in Fig. 1, the ceramic is covered with pure carbon.
II. SiC crystallites with an average size of 200 nm are embedded in an almost pure carbon matrix.
III. SiC crystallites with an average size of approx. 40 nm are embedded in a BNC matrix.

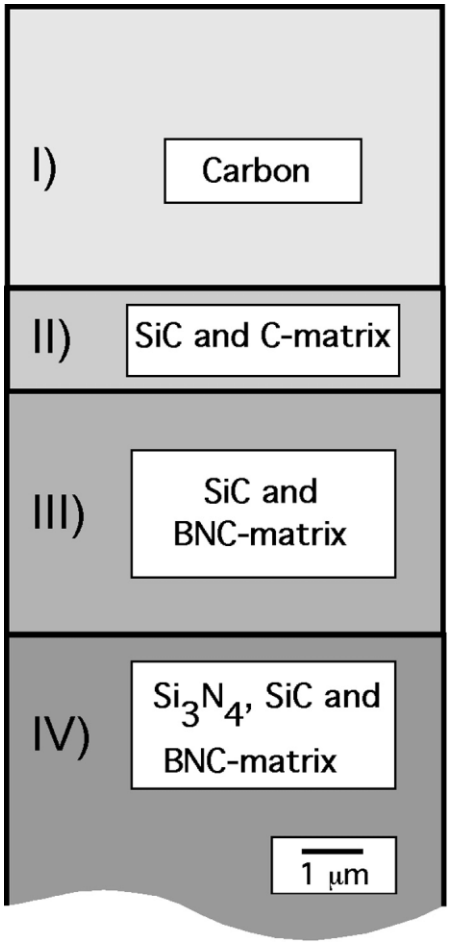

Fig. 5. Schematic drawing of the phase distribution at position 2 as a function of the distance from the crack.

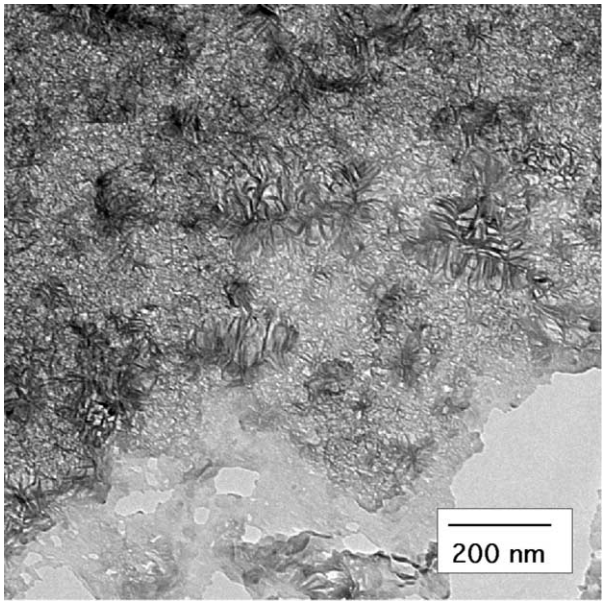

Fig. 6. TEM micrograph of the almost pure carbon in region I.

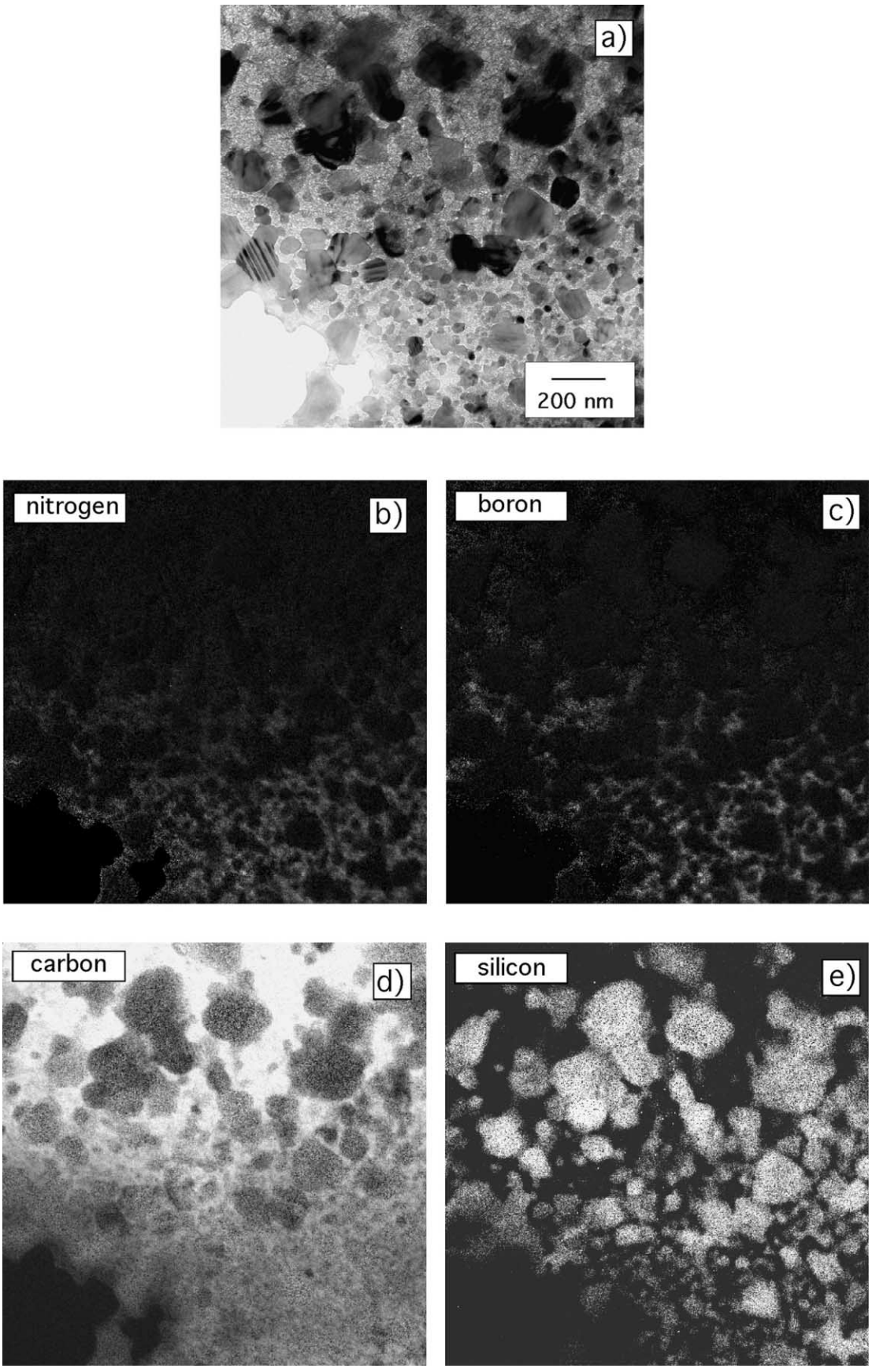

Fig. 7. Elemental maps of the interface of region II and III. (a) bright field image, (b) nitrogen, (c) boron, (d) carbon and (e) silicon.

IV. SiC and Si_3N_4 crystallites are embedded in a BNC matrix. This structure gradually evolves to the structure at position 1.

The lateral arrangement of these four regions is schematically shown in the shematic drawing in Fig. 5. Region I is the pure carbon layer. We estimate the thickness of region I to be at least 5 μm.

The thickness of region II is about 1.5 μm and that of region III is about 4 μm. The characteristic microstructures in these regions follow with a strict order of phases, as outlined above. Some selected TEM micrographs are shown in Figs. 6 and 7. Fiber-like structures can be seen in the micrograph in Fig. 6, which shows the pure carbon in region I. The fiber-like structures are typical for the turbostratic modification of carbon. In contrast to the graphitic modification of carbon which shows a well defined crystal structure consisting of planar layers with a stacking order ABA... (interplanar distance: 335 pm), the turbostratic modification of carbon exhibits interplanar distances in the range of 335–360 pm. This results in a less ordered structure which can also be confirmed with X-ray diffraction where reflexes (h,k,l) with $l \neq 0$ corresponding to the graphitic modification are absent or at least broadened very much. For more detailed information, see Ref. 23.

Fig. 7a shows the bright field image of the interface between the regions II and III. The upper part of the micrograph shows the large SiC crystallites of region II, embedded in the carbon matrix. In the lower part, the structure of region III can be seen. The lower part of the image shows the typical microstructure of the SiBCN ceramic. However, it has to be emphasised that no Si_3N_4 grains are present, which could be confirmed by taking the elemental maps shown in Fig. 7b–e, as well as by analysing diffraction patterns. Fig. 7b shows the nitrogen distribution of this area. Nitrogen is present only in the BNC matrix in the lower half of this figure. The boron distribution shown in Fig. 7c equals the nitrogen distribution. Fig. 7d shows the carbon distribution image in which pure carbon matrix of region II is bright (upper half of picture). Successively moving down to region III, a homogeneous grey value, indicating the decreasing carbon content of the BNC-matrix, can be seen. Fig. 7e shows the silicon distribution. Since all bright positions of Fig. 7e coincide always with grey positions of the carbon map Fig. 7d, all crystals of region II and III could be identified to consist of silicon carbide.

For a quantitative analysis of the atomic ratios of the elements boron, carbon and nitrogen present in the matrix, ESI series were acquired and evaluated. Fig. 8 shows the resulting atomic ratios of B/N, N/C and B/C in dependence of the distance from the crack. The origin of the abscissa has been positioned at the boundary of region I and II, since the thickness of region I is not

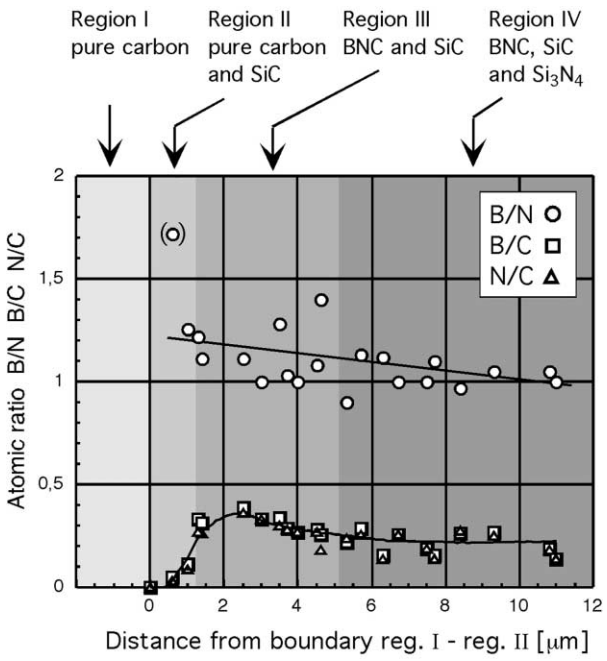

Fig. 8. Atomic ratio of the elements B, N and C of the matrix phase in dependence of the distance from the interface of regions I and II.

unique. It is observed that in all the B/N ratio remains almost constant at a value of slightly above 1, which is moderately increasing a towards the crack surface. The ratio of N/C reaches its maximum at a distance of 2.5 microns, which is approximately in the first half of region III. At this position the BNC-matrix showed the lowest carbon content and we measured a ratio B:C:N of 1.0:2.6:1.1. (For the regions see the legend of Fig. 8.) This behaviour can be explained by taking the degradation of silicon nitride to silicon carbide into account, which decreases the carbon content in the BNC matrix. For the given composition thermodynamical calculations yield a B:C:N ratio of 1.0:2.5:1.0. Only in the first half of region III experimentally determined values coincide well with thermodynamical calculations. It is also desirable that carbon was provided from region I via diffusion to increase the corresponding B:C:N ratio.

At a distance of 7–10 microns (region IV) we find a B:C:N ratio of 1.0:4.5:1.0, which means that the carbon content is somewhat higher than that of position 1 (Fig. 1).

The transition region between region III and IV shows an increasing presence of silicon nitride and no abrupt change in the ratio N/C or B/C is observed. Diffusion of the elements seems to smooth the curve.

4. Discussion and conclusions

Preparing ceramics from polymer precursors is a very promising method for processing covalently bonded ceramic materials. Due to the lack of oxide grain

boundary phases these materials offer high thermal and mechanical stability.

The turbostratic BNC matrix phase acts as a diffusion barrier for the carbon. Thus, the degradation of silicon nitride can be prevented up to temperatures of 2000 °C. Furthermore, the BNC-matrix inhibits the grain growth and the attractive nanocrystalline composite structures are stabilized up to elevated temperatures.

Our results represent the phase composition of the polymer-derived ceramics in the final stage. In order to reach this stage many processing steps are necessary. Each of these steps influences both final composition and microstructure of the material. One particulary important factor is the volume shrinkage and the resulting crack pattern during thermolysis of the material. The carbon layer at the crack surface (region I) most probably arises from CH_4 which is formed as a gaseous thermolysis product and in part decomposes into carbon and hydrogen whereby carbon is deposited at the crack surfaces.

An important result of our studies is that we measure a ratio of B:N of approximately 1:1 in the BNC-layers, independent from the individual carbon content. This supports the assumption that boron is preferentially bonded to nitrogen. Accordingly, the BNC matrix should be composed of pure boron nitride-layers in which pure graphite layers are interealated and vice versa. Further support comes from the results of Kohler-Redlich et al.[24] who found in BC_2N nanotubes the segregation of BN layers sandwiched between 'graphitic' C layers by using a dedicated STEM. Interestingly, the lowest carbon content of the BNC-matrix has not been found in the bulk, but rather in a small part of region III, mainly in the first half (Fig. 8, position 2.5 μm), where a ratio B:C:N of 1.0:2.6:1.0 is observed. This is the value expexted for an isolated ceramic material after decomposition of silicon nitride (theoretically: 1.0:2.5:1.0). At the interface of regions III and IV, the profiles of the atomic ratios show no discontinuity at this interface position. The high carbon content of region IV enriches the neighboring parts of region III with carbon. Thus, smooth profiles of the elemental ratios from B:C:N of 1.0:2.5:1.2 to 1.0:4.0:1.0 are observed.

Besides the complex behavior at the boundaries, the estimated phase amounts gathered from the bulk material at position 1 coincide very well with the predictions from thermodynamical calculations by Weinmann et al.[12]

Based on these results, further research items with respect to materials processing can be identified. One main item concerns the formation of cracks within the material which are due to the evolution of gaseous species and shrinkage up to 50 volume% during thermolysis. Therefore, research work has to focus on the development of new polymer systems with densities more closely to those of the corresponding ceramic materials in order to reduce the volume shrinkage. Moreover, precursors are desired that transform into ceramics in higher yield without formation of heavy volatile species but with exclusive formation of hydrogen that can disappear from the materials by diffusion processes. The increased diffusivity of hydrogen compared to other volatile species is especially interesting to produce dense and crack-free materials.

Acknowledgements

The authors thank the Deutsche Forschungsgemeinschaft (DFG) for financially supporting this work in the framework of the SPP precursor ceramic. We also thank Dr. Mehmet Gülgün for helpful discussion and revising this script, K. Hahn and U. Eigenthaler for their support at the Zeiss 912 Omega and D.C. Manocchio, U. Salzberger, M. Sycha and A. Strecker for their invaluable help in TEM sample preparation.

References

1. Riedel, R., Passing, G.., Schönfelder, H. and Brook, R. J., Synthesis of dense silicon-based ceramics at low temperatures. *Nature*, 1992, **355**, 714.
2. Bill, J. and Aldinger, F., *Adv. Mater*., 1995, **7**, 775–787.
3. Niihara, K., *J. Ceram. Soc. Jpn*., 1991, **99**, 974.
4. Riedel, R., Ruwisch, L., An, L. and Raj, R., *J. Am. Ceram. Soc*., 1998, **81**, 3341.
5. Jansen, M. and Baldus, H.-P. Ger. Offen. DE 410 71 08 A1, 1992.
6. Baldus, H.-P., Wagner, O. and Jansen, M., *Mater. Res. Soc. Symp. Proc*., 1992, **271**, 821.
7. Riedel, R., Kienzle, A., Petzow, G., Brück, M. and Vaahs, T. Ger. Offen. DE 432 07 83 A1, 1994.
8. Bill, J., Kienzle, A., Sasaki, M., Riedel, R. and Aldinger, F. In *Ceramics: Charting the Future*, ed. P. Vincenzini. Techna Sri, 1995.
9. Riedel, R., Kienzle, A., Dressler, W., Ruwisch, L. M., Bill, J. and Aldinger, F., *Nature*, 1996, **382**, 796.
10. Weinmann, M., Seifert, H.-J. and Aldinger, F., Boron containing non-oxide ceramics from organometallic polymers: synthesis, thermolysis and the influence of boron on materials thermal stability. In *Contemporary Boron Chemistry*, ed. M. G. Davidson, A. K. Hughes, T. B. Marder and K. Wade. The Royal Society of Chemistry, Cambridge, UK, 2000, pp. 88.
11. Baldus, H.-P. and Jansen, K., Moderne Hochleistungskeramiken—amorphe anorganische Netzwerke aus molekularen Vorläufern. *Angew. Chem.* **109**, 1997, 338–354 (*Angew. Chem. Int. Ed. Engl.* **36**, 1997, 328).
12. Weinmann, M., Schuhmacher, J., Kummer, H., Prinz, S., Peng, J., Seifert, H. J., Christ, M., Müller, K., Bill, J. and Aldinger, F., Synthesis and thermal behavior of novel Si–B–C–N ceramic precursors. *Chem. Mater*., 2000, **12**, 623–632.
13. Seifert, H. J., Lukas, B. H. L. and Aldinger, F., *Ber. Bunsenges. Physikal. Chemie*, 1998, **102**, 1309.
14. Seifert, H.-J. and Aldinger, F. In *Precursor-Derived Ceramics*, ed. J. Bill, F. Wakai and F. Aldinger. Wiley VCH, 1999, p. S.165.
15. Jalowiecki, A., Bill, J., Aldinger, F. and Mayer, J., Interface characterization of nanosized B-doped Si_3N_4/SiC ceramics. *Composites Part A*, 1996, **27A**, 717–721.

16. Reimer, L., Fromm, I. and Rennekamp, R., *Ultramicroscopy*, 1988, **24**, 339.
17. Mayer, J., Vinga Szabo, D., Rühle, M., Seher, M. and Riedel, R., Polymer-derived Si-based bulk ceramics, part II: microstructural characterisation by electron spectroscopic imaging. *J. Eur. Ceram. Soc*., 1995, **15**, 717–727.
18. Mayer, J., Eigenthaler, U., Plitzko, J. M. and Dettenwanger, F., Quantitative analysis of electron spectroscopic imaging series. *Micron*, 1997, **28**, 361–370.
19. Plitzko, J. M. and Mayer, J., Quantitative thin film analysis by energy filtering transmission electron microscopy. *Ultramicroscopy*, 1999, **78**, 207–219.
20. Strecker, A., Salzberger, U. and Mayer, J., *Pract. Metallography*, 1993, **30**, 482.
21. Strecker, A., Mayer, J., Gutekunst, G., Gemming, T., Eigenthaler, U., Baretzki, B. and Rühle, M., Optimization of TEM specimen preparation by double sided ion beam thinning under low angles. *Journal of Electron Microscopy*, 1999, **48**(3), 235–244.
22. D'Ans, Lax, *Taschenbuch für Chemiker und Physiker*, 4. Auflage, Springer Verlag, Band 3, 1998.
23. Baumgart, W. and Dunham, A. C., *Christian Amstutz: Process Mineralogy of Ceramic Materials*. Ferdinand Enke Verlag, Stuttgart, Germany, 1994.
24. Kohler-Redlich, Ph., Terrones, M., Manteca-Diego, C., Hsu, W. K., Terrones, H., Rühle, M., Kroto, H. W. and Walton, D. R. M., Stable BC_2N nanostructures: low-temperature production of segregated C/BN layered materials. *Chemical Physics Letters*, 1999, **310**, 459–465.